Available online at www.sciencedirect.com
ScienceDirect
Coastal Engineering 54 (2007) 618–629
Coastal Engineering
An International Journal for Coastal, Harbour and Offshore Engineers
www.elsevier.com/locate/coastaleng

Three-dimensional simulation of tsunami run-up around conical island

Byung Ho Choi [a,*], Dong Chule Kim [a], Efim Pelinovsky [b], Seung Buhm Woo [c]

[a] Department of Civil and Environmental Engineering, Sungkyunkwan University, Chunchun-dong 300, Jangan-gu, Suwon 440-746, Republic of Korea
[b] Institute of Applied Physics, Russian Academy of Sciences, 46 Uljanov Street, 603950, GSP-120, Nizhny Novgorod, Russia
[c] Department of Ocean Science, Inha University, Yonghyun-dong 253, Nam-gu, Incheon 402-751, Republic of Korea

Received 27 September 2006; received in revised form 23 January 2007; accepted 13 February 2007
Available online 21 March 2007

Abstract

At the circular Babi Island in the Flores tsunami (1992) and pear shaped island in the Okushiri event (1993), unexpectedly large tsunami run-up heights in the lee of conic islands were observed. The flume and basin physical model studies were conducted in the Coastal Hydraulic Laboratory, Engineering Research and Development Center, U.S. Army Corps of Engineers to provide a better understanding of the physical phenomena and verify numerical models used in predicting tsunami wave run-up on beaches, islands, and vertical walls. Reasonably accurate comparison of run-up height of solitary waves on a circular island has been obtained between laboratory experimental results and two-dimensional computation model results. In this study we apply three-dimensional RANS model to simulate wave run-up on conical island. In the run-up computation we obtain that 3D calculations are in very good comparison with laboratory and 2D numerical results. A close examination of the three-dimensional velocity distribution around conical island to compare with depth-integrated model is performed. It is shown that the velocity distribution along the vertical coordinate is not uniform: and velocity field is weaker in the bottom layer and higher on the sea surface. The maximum difference (about 40%) appears at the time when solitary wave reached the circular island.

Keywords: Tsunami; Conical island; Three-dimensional computation model

1. Introduction

In the Flores Island tsunami (1992) at the circular shaped Babi Island and pear shaped Okushiri tsunami events (1993), unexpectedly large tsunami run-up heights in the lee of small islands were observed and huge human and material losses were incurred. (Liu et al., 1991; Liu et al., 1995a,b; Cho, 1995; Yeh et al., 1996). Recently a similar run-up process was believed to occur at Car Nicobar Island close to 2004 December Sumatra–Andaman earthquake source region (Choi et al., 2006). This characteristic phenomenon initiated a lot of experimental and theoretical studies.

Laboratory experiments were performed in a large-scale basin at the Coastal and Hydraulics Laboratory (hereinafter referred as CHL), US Army Corps of Engineers (Briggs et al., 1994). The basin was 30 m wide and 25 m long. A circular island is located on the center of the basin. A directional spectral

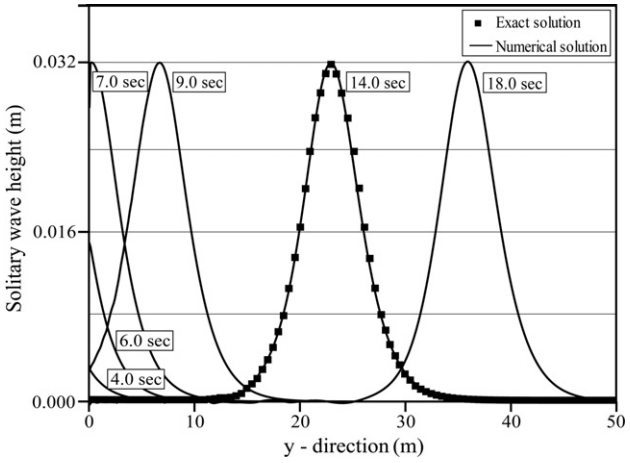

Fig. 1. Comparison of solitary wave propagation between the exact solutions and numerical solution.

* Corresponding author. Laboratory for Coastal and Ocean Dynamics Studies, Department of Civil and Environmental Engineering, Sungkyunkwan University, Chunchun-dong 300, Jangan-gu, Suwon 440-746, Republic of Korea. Tel.: +82 31 290 7534; fax: +82 31 290 7549.
E-mail addresses: bhchoi@yurim.skku.ac.kr, bhchoi@skku.edu (B.H. Choi).

0378-3839/$ - see front matter © 2007 Elsevier B.V. All rights reserved.
doi:10.1016/j.coastaleng.2007.02.001

Table 1
Conditions of the numerical model experiments

Solitary wave		Rayleigh method by Katell and Eric (2002)
Depth		0.32 m
Amplitude of solitary wave		0.016 m/0.032 m/0.064 m: 3 cases
Cell	*x* direction	Total cell: 360 (maximum cell size 0.19 m, minimum cell size 0.05 m)
	y direction	Total cell: 330 (maximum cell size 0.19 m, minimum cell size 0.05 m)
	z direction	Total cell: 19 (maximum cell size 0.04 m, minimum cell size 0.04 m)
	Total	Computed cell number=2,257,200 cells (30 m×25 m×0.76 m)
Turbulent computation		Renormalized group (RNG) model

wave generator (DSWG) was installed along the *x*-axis and was used to generate solitary waves. Four DWSG were employed to generate incident solitary waves with different crest lengths. These laboratory results were provided as a benchmark problem of run-up simulations and a series of numerical experiments were reported using various numerical schemes however model applications were limited to two-dimensional. Among these model simulations, Liu et al. (1994, 1995a,b) and Cho and Liu (1999) developed a numerical model based on the two-dimensional nonlinear shallow-water equations to describe the propagation and run-up of solitary waves. They discretized the governing equations with a finite difference method and employed a first-order accurate upwind scheme to analyze the

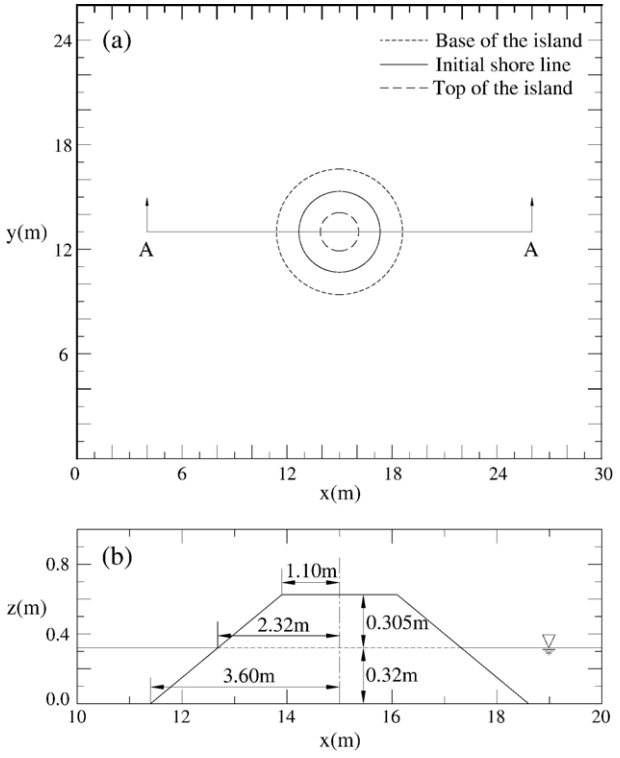

Fig. 2. Top view of the wave basin and the island (upper) and vertical view of the island on the cross-section A–A (lower).

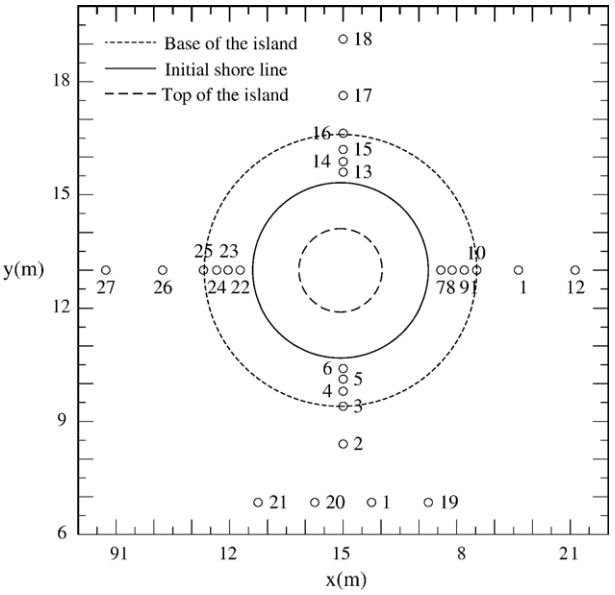

Fig. 3. Locations of wave gauges.

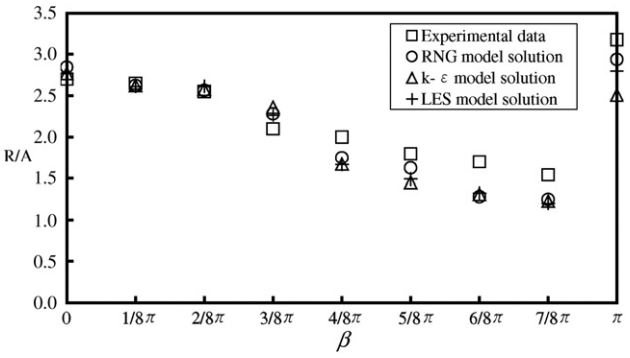

Fig. 4. Comparison of normalized maximum run-up height distribution around the circular island: □ Briggs et al. (1994) experimental data; ○ RNG model solution, Δ *k*–ε model solution and + LES model solution.

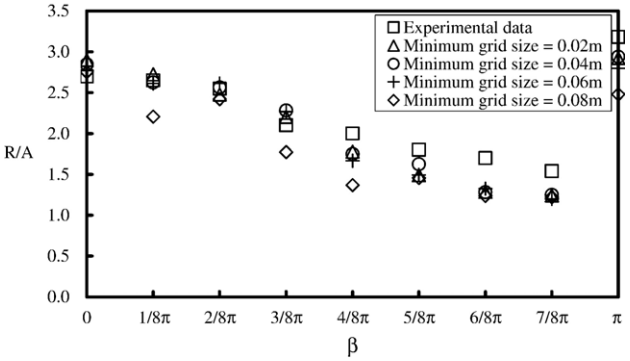

Fig. 5. Comparison of normalized maximum run-up height distribution around the circular island: □ Briggs et al. (1994) experimental data; Δ minimum grid size=0.02 m, ○ minimum grid size=0.04 m, + minimum grid size=0.06 m, ◇ minimum grid size=0.08 m.

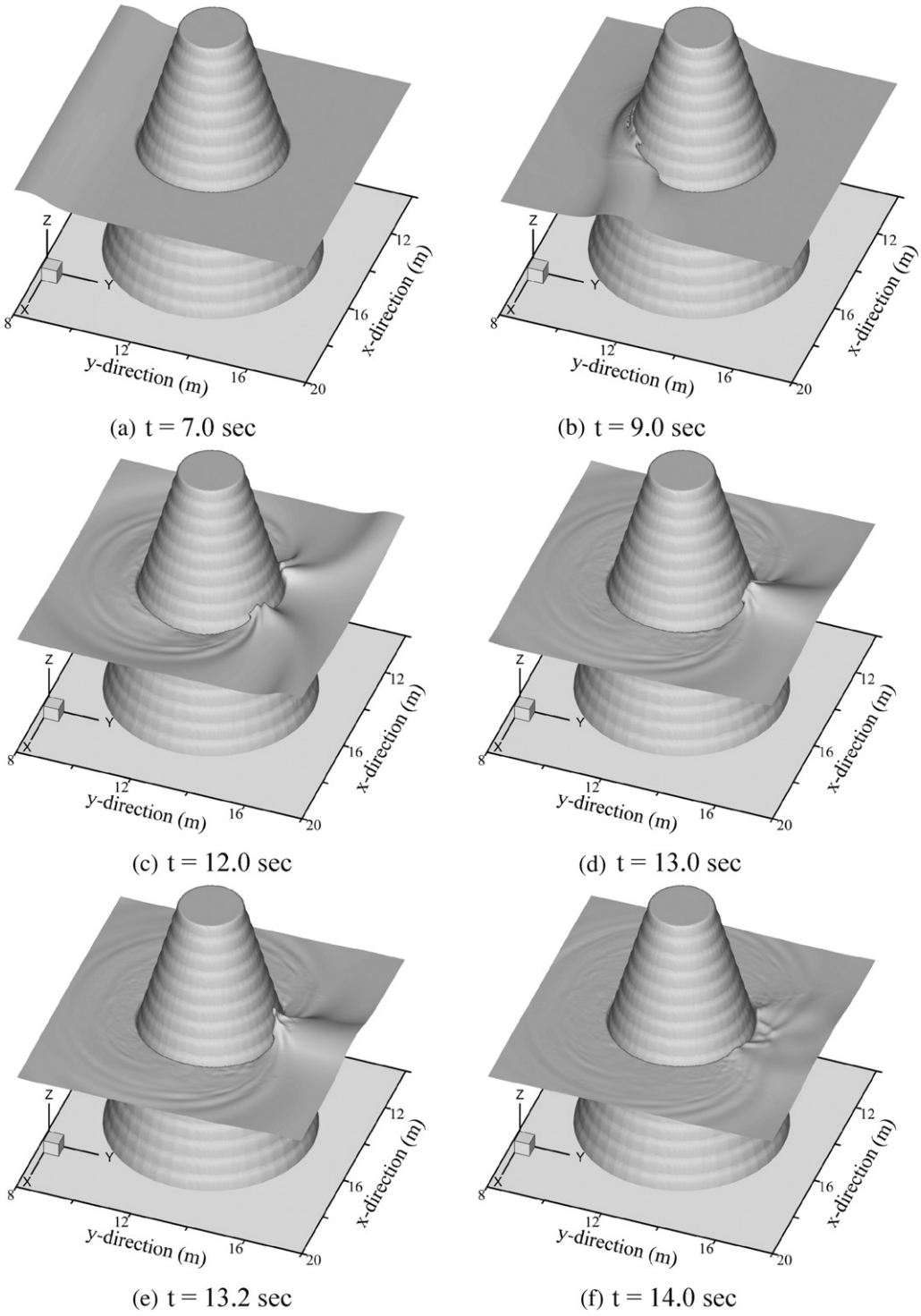

Fig. 6. Snapshots of free surface at different times for $\varepsilon = 0.10$.

nonlinear convection terms of the momentum equations. Obtained results agreed well with laboratory measurements carried out by CHL.

In this study, an adaptive RANS 3D model was employed to investigate the run-up heights of near shore tsunami around a circular island. Numerical model is described in Section 2. Simulations were done for the same conditions which were used in laboratory measurements done at the CHL (Briggs et al., 1994). The newly obtained maximum run-up heights will be compared with these laboratory and numerical results of Liu et al. (1995a,b); these results are presented in Section 3. It is obtained that 3D calculations are in very good comparison with laboratory and 2D numerical results. Results of the calculation of the 3D velocity field are described in Section 4. The velocity

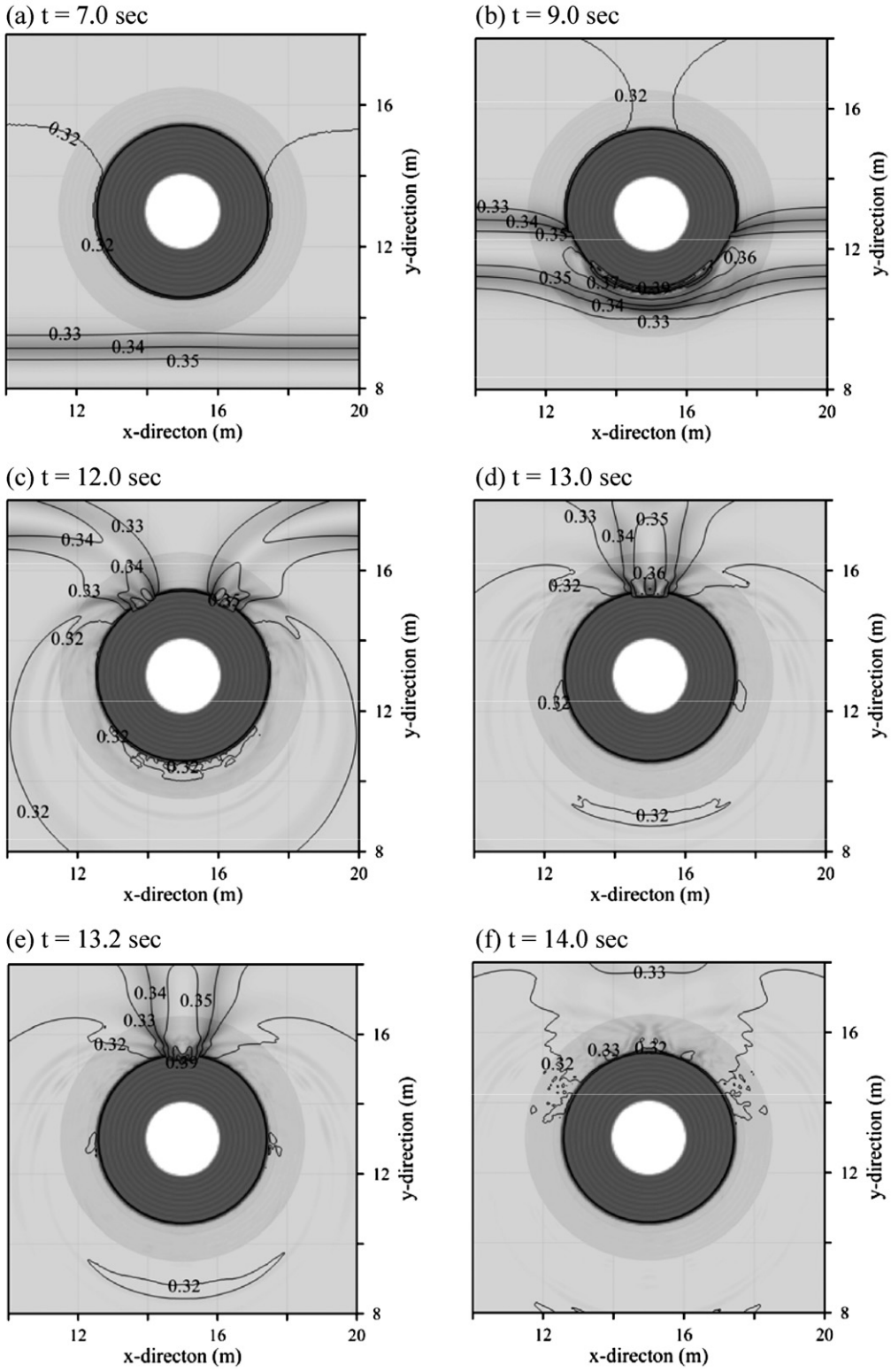

Fig. 7. Contours of the water level displacement for $\varepsilon = 0.10$ (in meters) around the island (maximum lee-side run-up = 0.0414 m).

distribution along the vertical coordinate is not uniform: and velocity field is weaker in the bottom layer and higher on the sea surface. This conclusion is inconsistent with the basic assumption of the depth-averaged equation model where the horizontal velocity is uniform in depth. The difference is maximal at the time of solitary wave approaching to the island. The results of the computing of the turbulent dissipation are presented in Section 5. It is shown that wave energy impact on the land could be reasonably explained in a 3D model. In our opinion it explains why the lee side of the island is so much damaged by the tsunami, as we have seen in the Babi Island (1992 Flores Tsunami).

2. Numerical model

2.1. FLOW-3D model

A well-known computational technique was developed by Hirt (1994), and was implemented in the CFD code, FLOW-3D. The program solves the Navier–Stokes equation by the finite difference method. It utilizes a true volume of fluid method for computing free surface motion (Nichols et al., 1980; Hirt and Nichols, 1981) and the fractional area/volume obstacle representation (FAVOR) technique to model complex geometric regions (Hirt and Sicilian, 1985). The true VOF method tracks the sharp interface accurately and does not compute the dynamics in the void or air regions. The portion of volume or area occupied by the obstacle in each cell (grid) is defined at the beginning of the analysis. The fluid fraction in each cell is also calculated. The continuity, momentum or transport equation of fluid fraction is formulated using the FAVOR function. A finite difference approximation is used for discretization of each equation. Unlike some finite element/volume or boundary fitting grid methods, this meshing technique does not require re-meshing and would not induce any mesh distortion during transient analysis. Hence an accurate solution algorithm can be applied easily.

Furthermore, multi-block meshing technique can be employed to provide higher resolution of simulation in the region of interest if necessary. The basic algorithm for advancing a solution in a one time increment consists of the following three steps (Flow Science, 2002):

1. Compute the velocities in each cell using the initial conditions or previous time-step values for all advective pressure, and other accelerations based on the explicit approximations of the momentum (Navier–Stokes) equations.
2. Adjust the pressure in each cell to satisfy the continuity equation.
3. Update the fluid free surface or interface to give the new fluid configuration based on the volume of fluid value in each cell.A mixture of explicit and implicit solution schemes can be used to solve for the partial differential equations. The selection depends on the complexity of the fluid flow problem in question. Detailed information is described in Versteeg and Malalasekera (1995).

Table 2
Normalized maximum run-up heights around the circular island ($\varepsilon = 0.05$)

Location	Experimental data	2D numerical solutions	3D numerical solutions
0	2.600	2.700	2.950
1/8π	2.580	2.390	2.731
2/8π	2.520	2.520	2.388
3/8π	2.150	2.150	2.319
4/8π	1.980	1.810	1.775
5/8π	1.590	1.590	1.313
6/8π	1.530	1.530	1.238
7/8π	1.250	1.080	1.106
π	2.000	2.100	2.531

Table 3
Normalized maximum run-up heights around the circular island ($\varepsilon = 0.10$)

Location	Experimental data	2D numerical solutions	3D numerical solutions
0	2.700	2.880	2.844
1/8π	2.650	2.500	2.625
2/8π	2.550	2.380	2.563
3/8π	2.100	2.350	2.281
4/8π	2.000	2.160	1.750
5/8π	1.800	1.780	1.625
6/8π	1.700	1.440	1.281
7/8π	1.540	1.370	1.250
π	3.180	2.520	2.938

2.2. Boundary condition for solitary wave generation

Although various types of boundary conditions (BC), including slip/no-slip wall BC, moving solid BC and open BC, were equipped in the FLOW-3D, the incident wave BC has to be introduced to generate a certain type of wave that we are interested in, which is the solitary wave in this study. Two different ways of implementing incident wave BC were tested: one way is simulating the movement of a Piston-type wave-maker using the moving solid wall BC and the other way is using the free surface elevation and velocity field derived from the theoretical solutions.

For the case of using moving solid wall BC, we have tested various wave-maker methods suggested by Katell and Eric (2002). Among those methods, we found that the Rayleigh method with the modification of Piston-type wave-maker is the most acceptable. This procedure can be explained in the following way. The solid wall (paddle) position is defined along the x-axis in the form

$$\frac{dX}{dt} = \overline{u}(X,t) \tag{1}$$

where X is the paddle position, and u the depth-averaged velocity, and X is suggested by Katell and Eric (2002) under the small amplitude assumption such that

$$X(t) = \frac{2Ah\ \tanh\left(\frac{t}{2}\sqrt{\frac{3gA(A+h)}{h^2(A+h)}}\right)}{h\sqrt{\frac{3A}{h^2(A+h)}}\left\{h + A\left[1 - \tanh^2\left(\frac{t}{2}\sqrt{\frac{3gA(A+h)}{h^2(A+h)}}\right)\right]\right\}} \tag{2}$$

where, A is the wave amplitude, and h is the depth. In the numerical code, the position of solid wall is defined at each time step following Eq. (4).

Table 4
Normalized maximum run-up heights around the circular island ($\varepsilon = 0.20$)

Location	Experimental data	2D numerical solutions	3D numerical solutions
0	2.850	2.240	2.888
1/8π	2.750	2.100	2.827
2/8π	2.580	1.700	2.627
3/8π	2.250	1.750	2.277
4/8π	1.780	1.450	1.666
5/8π	1.200	0.900	1.208
6/8π	0.810	0.950	0.861
7/8π	0.650	0.900	0.691
π	1.840	1.500	1.953

Although this way of wave generation is consistent in a physical sense, it causes the numerical solution unstable. To avoid the numerical instability, the grid resolution should be very high, i.e.,

$$\frac{\Delta x}{\lambda} \leq \frac{1}{500}$$

(Cho, 1995), where λ is the wave length. Otherwise the solitary wave shape is deformed from the beginning and finally the solution is unstable.

It is found that the other way of generating solitary wave, i.e., specifying free surface and velocity field is better than using moving solid wall BC, since it is easier to implement, computationally less expensive and stable. Although there exist various types of solitary wave solutions with slightly different accuracy, we adopted the Boussinesq solution for this study. In particular, the weak-amplitude solitary wave solution, derived from Boussinesq equations, can be expressed as:

$$\eta(x,t) = A\,\mathrm{sech}^2\left[\sqrt{\frac{3A}{4h^3}}\,(x-ct)\right] \tag{3}$$

where η is the free surface elevation, h the still water depth, H the wave height, and

$$c = \sqrt{g(h+A)}$$

the wave celerity. The corresponding velocity field can be given as:

$$u = c\left\{\left[\frac{A}{h} + 3\left(\frac{A}{h}\right)^2\left(\frac{1}{6} - \frac{1}{2}\left(\frac{z}{h}\right)^2\right)\right]\frac{\eta}{A} - \left(\frac{A}{h}\right)^2\left(\frac{7}{4} - \frac{9}{4}\left(\frac{z}{h}\right)^2\right)\left(\frac{z}{A}\right)^2\right\},$$
$$v = 0,$$
$$w = c\sqrt{\frac{3A}{h}}\frac{z}{h}\frac{\eta}{h}\tanh\left[\sqrt{\frac{3A}{4h^3}}(x-ct)\right]\left\{1 + \frac{A}{2h}\left[1 - 7\frac{\eta}{A} - \left(\frac{z}{h}\right)^2\left(1 - \frac{3\eta}{A}\right)\right]\right\}. \tag{4}$$

Fig. 1 shows that such solution is stable and has no additional tails.

2.3. Computational domain

The computational domain used in this study is the same as the one used in the hydraulic experiment done by Briggs et al. (1994). The water tank is $x=30$ m, $y=25$ m, $z=0.76$ m, and the grid size and other experimental conditions are as those in Table 1. The geometry of the island in the basin system is symmetrical with respect to the line passing through the island center and perpendicular to the crests of incident waves (Fig. 2). Time histories of free surface displacements were measured at 27 different locations (Fig. 3).

3. Run-up computation

It is shown in Fig. 4 that numerical simulations of different turbulent models (k–ϵ, RNG (Renormalization Group) theory, LES (Large Eddy Simulation)) are done as other simulation conditions are same. Results of R/A (run-up height/initial wave height) were compared at each turbulent model simulation that are largely similar. But, result of the k–ϵ is under-estimated at the lee side of the island. In many previous studies, LES simulation result is most accurate among others at any complicated case and RNG model is more accurate than k–ϵ model. In this study, LES model and RNG model compute largely similar results. Generally, the RNG model has a wider applicability than the standard k–ϵ model. In particular, the RNG model is known to describe more accurately for low intensity turbulence flows and flows having strong shear regions (Yakhot and Orszag, 1986).

Adopting RNG model for computational efficiency, test has been done for different grid size as shown in Fig. 5, and showed the convergence of the model result. The minimum grid size adopted in this study is 0.04 m ($-z$ direction). Results of R/A (run-up height/initial wave height) were compared at each minimum grid size 0.02 m, 0.04 m, 0.06 m, 0.08 m that are largely similar except at 0.08 m. Case of the 0.08 m grid size has relatively large error, difference with the others and experimental data. Grid damping has occurred at a large minimum grid size but the adopted minimum grid size in this study is agreeable.

Fig. 6 shows the typical snapshots of the free surface at different times of solitary wave approaching to the conical island (initial amplitude/depth is $\varepsilon=0.1$). The formation of a big wave on the opposite side of the island is clearly seen. It can be interpreted as the superposition (collision) of two waves moving around the different sides of the island. The same process is

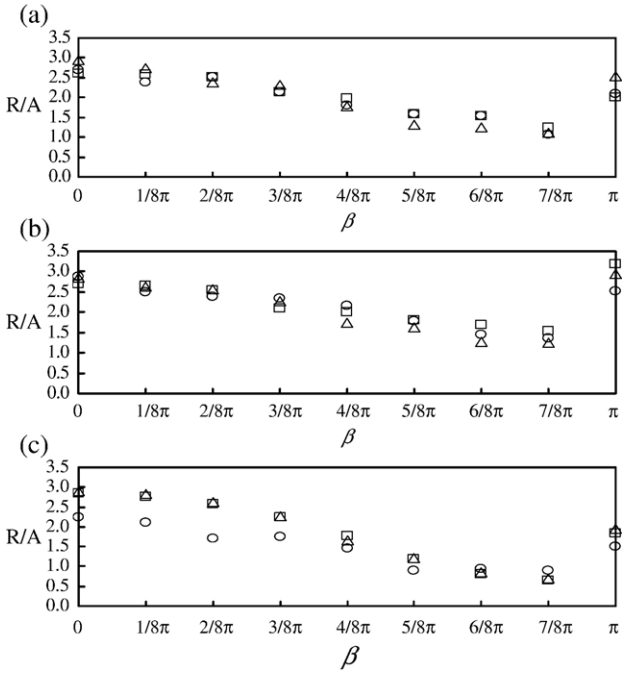

Fig. 8. Comparison of normalized maximum run-up height distribution around the circular island: (a) $\varepsilon=0.05$. (b) $\varepsilon=0.10$, (c) $\varepsilon=0.20$; □ Briggs et al. (1994) experimental data; ○ Liu et al. (1995a,b) 2D numerical solutions and □ present study 3D numerical solutions.

illustrated by Fig. 7; where the contours of the sea surface displacement are given. Qualitatively, same results were obtained in experiments (Briggs et al., 1994) and two-dimensional computing (Liu et al., 1995a,b). The comparison of conducted 3D calculations with laboratory and 2D numerical simulations is presented in Table 2–4 and Fig. 8 for the three values of initial amplitude/depth, ε: 0.05, 0.1, and 0.2 (initial depth is 0.32 m for all computations). Here the amplification (shoaling) factor (R/A) is given for the characteristics of the wave run-up (R is the run-up height, and A is the incident solitary wave height). The angle $\beta=0$ corresponds to the front direction of the wave approaching and $\beta=\pi$ as the back direction. As a whole, our 3D calculations are in a very good comparison with laboratory and 2D numerical results. Best agreement of computed run-up height around the conical island with laboratory data is obtained for the large-amplitude wave

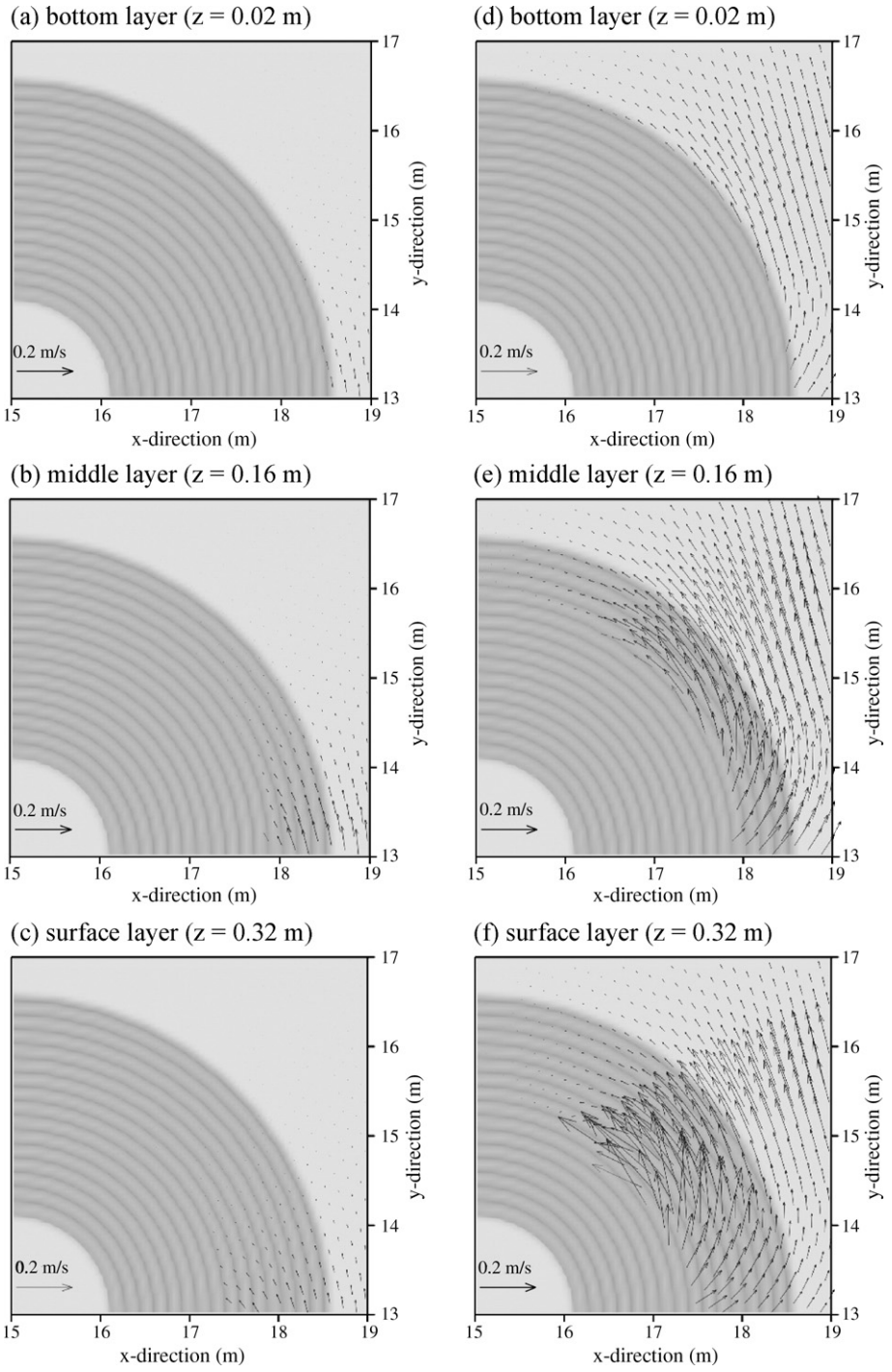

Fig. 9. (1) Horizontal velocity distribution at different times and depths (a), (b), (c): $t=9.0$ s; (d), (e), (f): $t=11.0$ s. (2) Horizontal velocity distribution at different times and layers (a), (b), (c): $t=12.0$ s; (d), (e), (f): $t=12.5$ s.

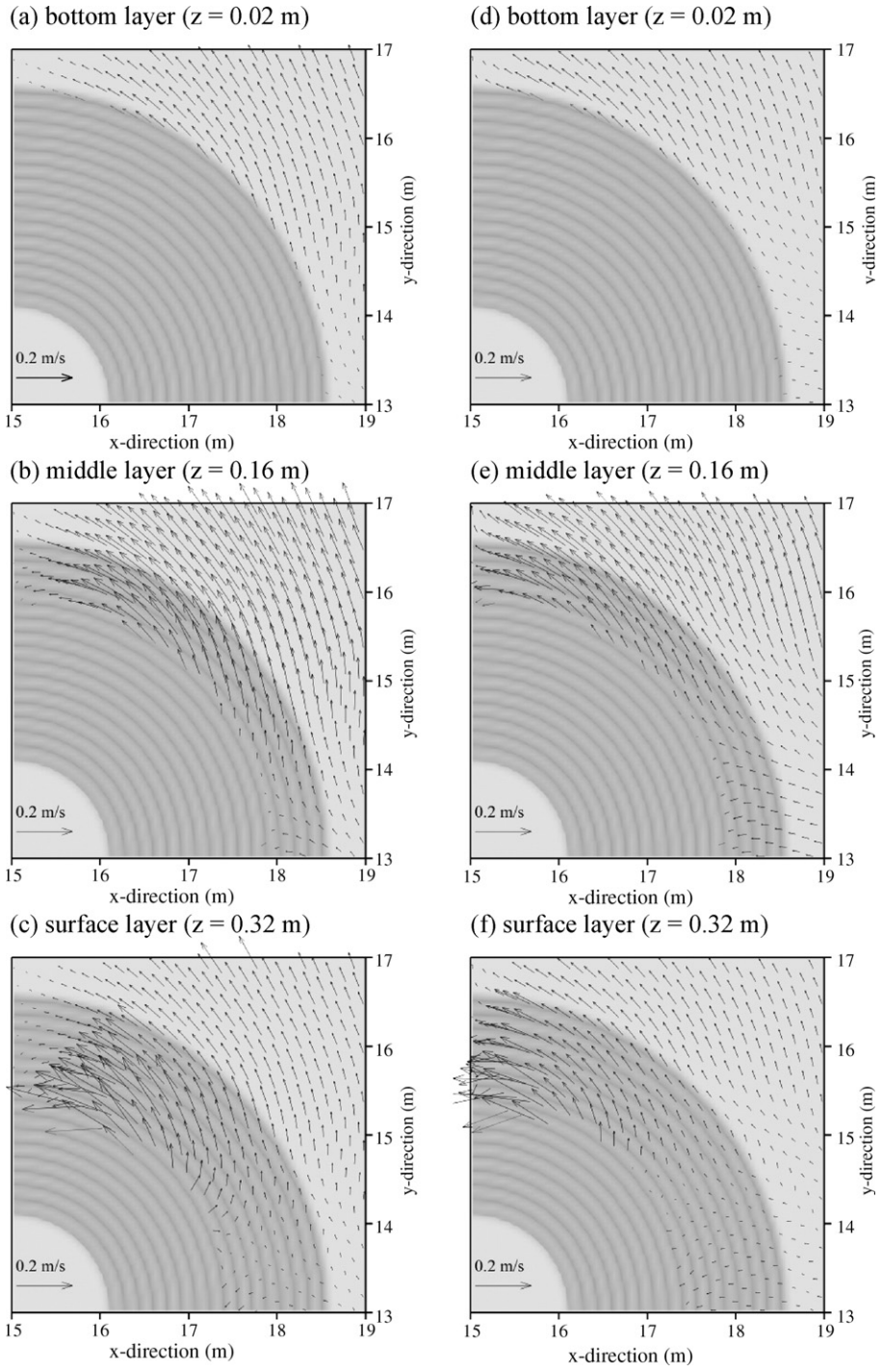

Fig. 9 (*continued*).

(ε=0.2), and the difference in magnitudes does not exceed 6% (ε=0.05:<21%, ε=0.1:<9%).

4. Velocity distribution

Fig. 9 shows the spatial distribution of the horizontal velocity field in the lee side of the island on various depths for four times: from 9.0 s, when the solitary wave approached the front of the island, to 12.5 s, when the maximum run-up height on back side of the island is achieved. As it is clearly seen, the velocity distribution along the vertical coordinate is not uniform: and the velocity field is weaker in the bottom layer and higher on sea surface. This conclusion is inconsistent with the basic assumption of the depth-averaged equation model where the horizontal velocity is uniform in depth. Therefore even though the maximum run-up height comparison does not show much difference between 2D and 3D model, it does not necessarily mean that the flow pattern is correctly simulated.

The 3-dimensional feature of the run-up process can be clearly shown from the vertical velocity profile as shown in

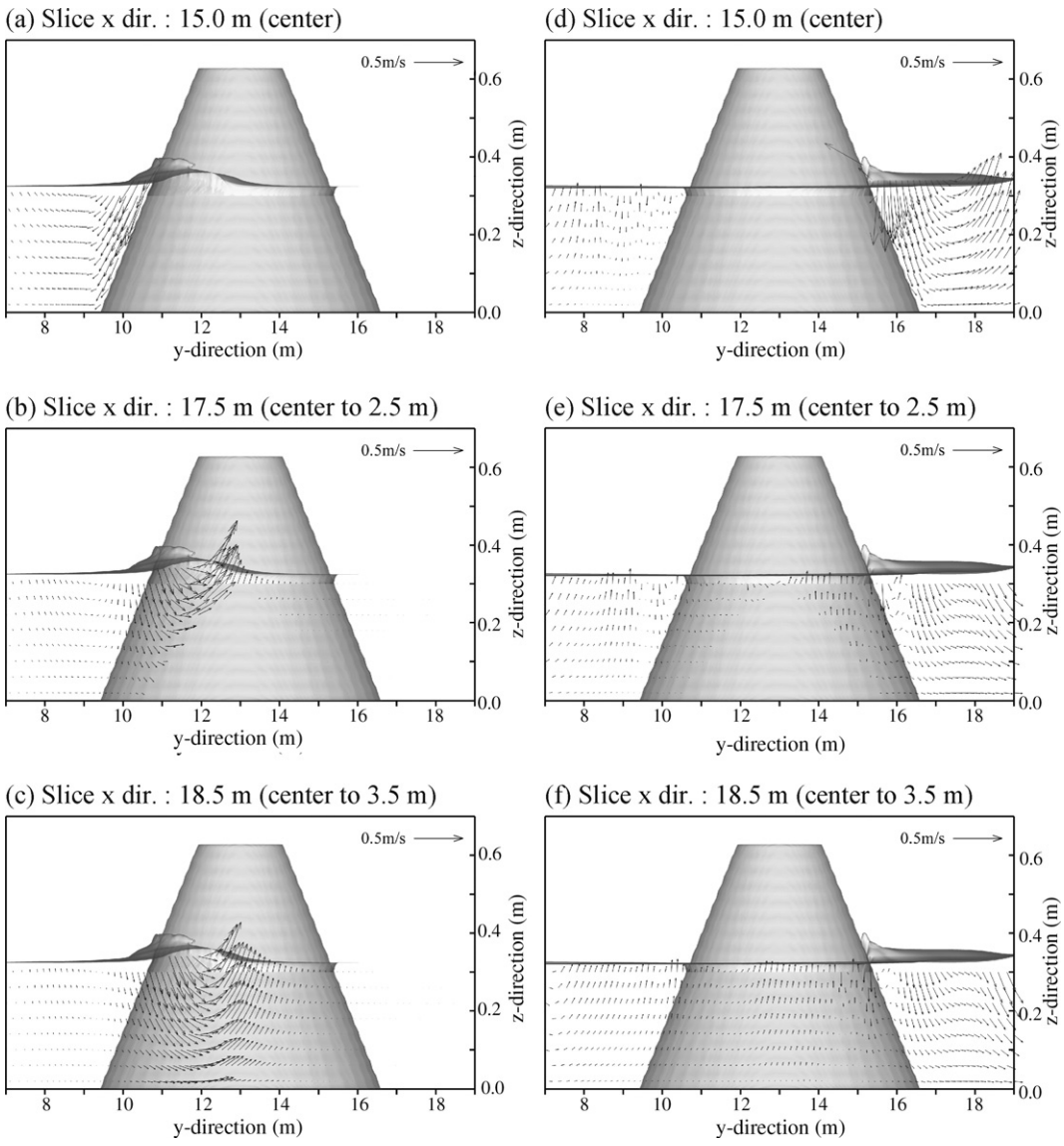

Fig. 10. Vertical velocity distribution at different cross sections (a), (b), (c): t=9.0 s; (d), (e), (f): t=13.2 s.

Fig. 10. It shows vertical velocity at the lee side of the island at t=13.2 s. A strong vertical velocity is shown at the front and back sides of the island and these patterns are shown even further downstream. These results implies that the assumption of the depth-averaged 2D model – the order of magnitude of the vertical velocity intensity is lower than that of horizontal velocity – is not a proper one for the conical run-up case. A strong vertical velocity profile could be directly related to the uplifting force that caused a severe damage on artificial structure.

The difference in 2D and 3D simulations can be characterized quantitatively by the "mean-square error" parameter

$$[\kappa(z_l,t)]^2 = \frac{\sum(|\vec{u}(x,y,z_l,t)| - |\vec{u}(x,y,z_{\mathrm{sur}},t)|)^2}{\sum|\vec{u}(x,y,z_{\mathrm{sur}},t)|^2} \quad (5)$$

which characterized the difference in the velocity field on depth l to compare with the surface field. The sum in Eq. (5) is over all computed points on fixed depth. It is evident that for the depth-averaged model this parameter κ^2=0 (Pelinovsky et al., 1999).

Table 5
2D and 3D computational results comparison parameter κ^2 at different times and layers

Layer		Time						
		7 s	9 s	11 s	12 s	13 s	13.5 s	14 s
Bottom layer	κ^2	0.00432	0.37385	0.41298	0.33400	0.21633	0.10689	0.12021
Middle layer	κ^2	0.00202	0.26593	0.27806	0.22813	0.14334	0.07376	0.08991

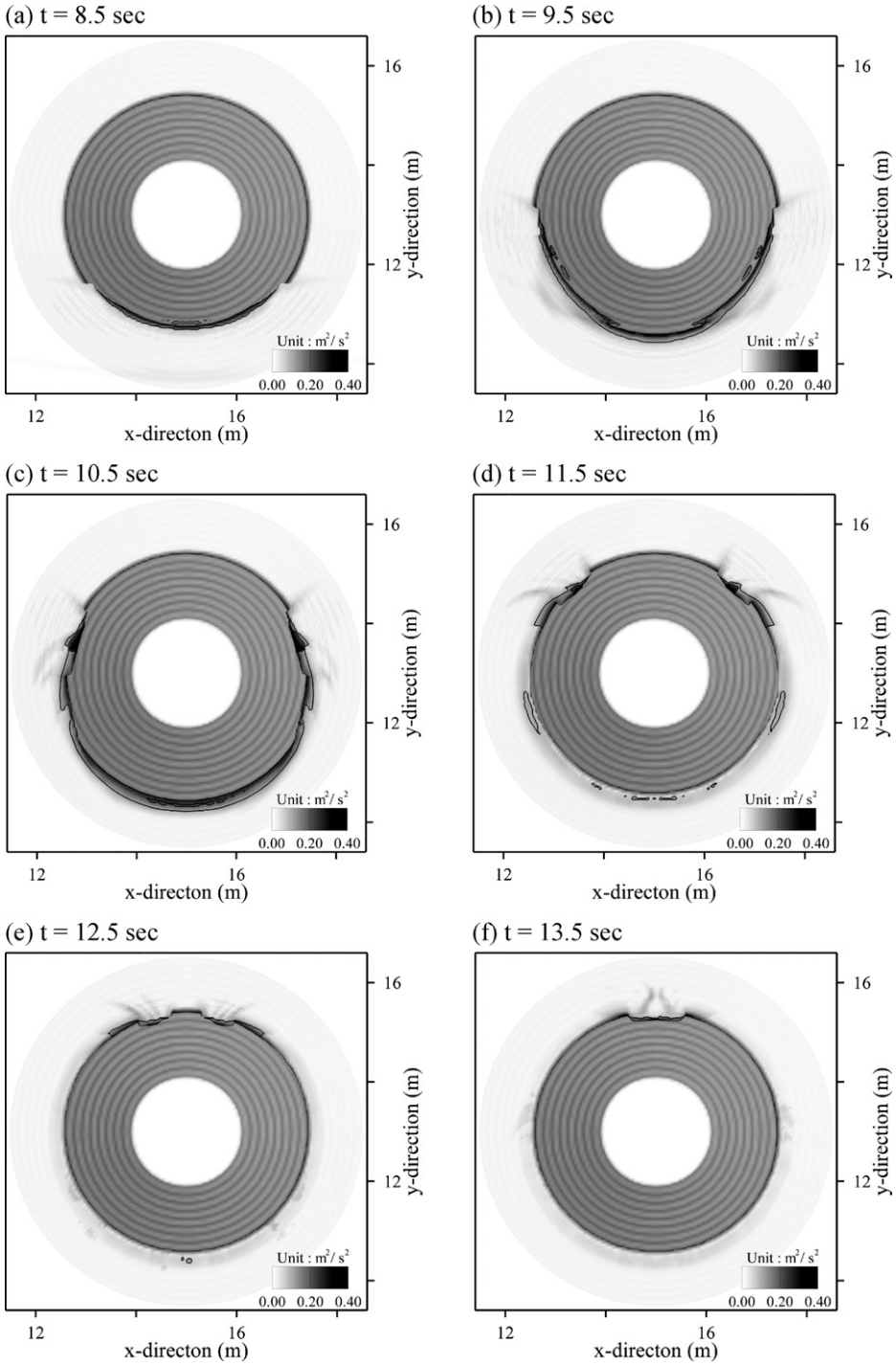

Fig. 11. Dissipation of kinetic turbulent energy around the island.

The computed results of the mean-square error are presented in Table 5. The maximum value (41%) appears in the bottom layer at 11 s and it is the time when wave propagates at the lee side of the island. The second maximum value (37%) appears in the bottom layer at 9 s and it is the time when run-up does occur in front of the island as a solitary wave reaching to the circular island. In this moment the vertical distribution of the velocity field is strongly non-uniform. The difference between 2D and 3D computations remains to be not weak for all the moments of the wave interaction with an island (about 10% for $t=14$ s).

5. Turbulent dissipation

The three-dimensional turbulent structure of the solitary wave over the circular island can be investigated from the present numerical simulation, where the RNG turbulence closure combined with the VOF surface tracking method is

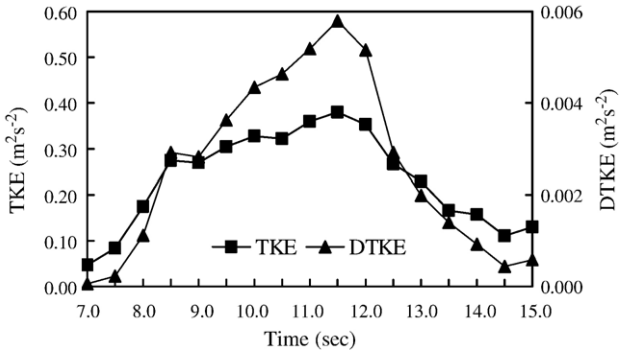

Fig. 12. TKE and DTKE around the island at different times.

adopted. The accuracy of turbulent simulation using this method is already verified by several previous studies (Rodriguez et al., 2004).

If the Reynolds-averaged Navier–Stokes (RANS) equations are solved, a variety of turbulent closures can be chosen, including a mixing length theory, one equation model, two equation (k–ε) models and Renormalization Group Theory (RNG). This last closure represents an improvement over the standard k–ϵ model – widely used in computational hydraulics during the seventies – and performs better in situations of high shear and separation zones. The RNG turbulent closure is represented by the following transport equations for turbulent kinetic energy (Eq. (6)) and turbulent dissipation (Eq. (7)):

$$\frac{\partial k}{\partial t} + u_i \frac{\partial k}{\partial x_j} = \nu_t \left(\frac{\partial u_i}{\partial x_j} + \frac{\partial u_j}{\partial x_i} \right) \frac{\partial u_i}{\partial x_j} + \frac{\partial}{\partial x_j} \left(\alpha_k \nu_{\text{eff}} \frac{\partial k}{\partial x_j} \right) - \varepsilon \tag{6}$$

$$\frac{\partial \varepsilon}{\partial t} + u_j \frac{\partial \varepsilon}{\partial x_j} = c_{\varepsilon 1} \frac{\varepsilon}{k} \nu_t \left(\frac{\partial u_i}{\partial x_j} + \frac{\partial u_j}{\partial x_i} \right) \frac{\partial u_i}{\partial x_j} + \frac{\partial}{\partial x_j} \left(\alpha_\varepsilon \nu_{\text{eff}} \frac{\partial \varepsilon}{\partial x_j} \right) - c_{\varepsilon 2} \frac{\varepsilon^2}{k} - R \tag{7}$$

with

$$\nu_{\text{eff}} = \nu_t \left[1 + \sqrt{\frac{c_\mu k}{\mu \sqrt{\varepsilon}}} \right]^2$$

$$\eta = \sqrt{\left(\frac{\partial u_i}{\partial x_j} + \frac{\partial u_j}{\partial x_i} \right) \frac{\partial u_i}{\partial x_j} \frac{k}{\varepsilon}}$$

where ν_t is the eddy viscosity, μ is the dynamic viscosity of the fluid and $c_{\varepsilon 1}$, $c_{\varepsilon 2}$, c_3, α_k, α_ε, η_0 and c_μ are constants. The RNG theory predicts $c_{\varepsilon 1}=1.42$, $c_{\varepsilon 2}=1.68$, $c_3=0.012$, $\eta_0=4.38$ and $c_\mu=0.085$, whereas α_k and α_ε are of order 1. In this model, turbulence is more sensitive to the mean rate of strain than the standard k–ε model, due to the presence of the term R.

We aim to investigate the mechanism of turbulent kinetic energy (TKE) generation and dissipation during the solitary wave impact. We also focus on when and where the maximum turbulent kinetic energy (TKE) concentration occurs. This understanding would be the basis for the explanation of why the most severe damage occurred at both lee-side edges of the conic island, as was observed in the Babi Island in the 1992 Flores Tsunami.

The snapshots of spatial TKE distribution of the surface layer at the island are shown in Fig. 11. TKE is initially generated at the front of the island and continuously propagated along the perimeter following the main wave. Two opposite directional flows, which are refracted around the island, strongly collide together at the lee side of the island. This suggests that the strongest turbulent energy generation/dissipation due to the collision of the flow could happen at the very lee of the island.

During the impact on the island, wave energy is supposed to be the strongest near the surface due to the turbulent flow. The simulation results tell us that the intensity of TKE is strongest at the surface and rapidly decays downward. If the wave energy diminishes due to turbulence, then it could explain why the run-up height in 3D and 2D show similar results although the flow intensity is fairly different. The intensity of flow velocity in the 3D model is much stronger than the 2D especially at the surface region, where a certain amount of wave energy is dissipated due to turbulence. This energy dissipation (momentum loss) prevents run-up height from being overestimated. Therefore, although the numerical results of maximum run-up height along the island are similar between 2D and 3D models, the simulation of wave energy impact on the land could be reasonably explained by 3D model only.

The time variation of the total turbulent kinetic energy (TKE) and dissipation of turbulent kinetic energy (DTKE) values at the surface layer are shown in Fig. 12. It shows that TKE and DTKE values increase as the wave propagates in front of the island until around 11.5 s. After having its maximum value at 11.5 s, the total TKE is reduced during the passing through the island. At 13.5 s, when the maximum run-up height is generated at the very lee of the island, the total TKE is smaller than its maximum.

The maximum TKE is generated around 11.5 s, at which time the major surface TKE is located at the lee-side left/right edge as shown in Fig. 11. Thus, location at which the maximum turbulence is generated is at the lee-side left/right edge of the conic island, not at the very lee of the island. Therefore, the lee-side edge of the island can be regarded as the most vulnerable place of the conical island, since the actual damage on the island could be measured by the intensity of TKE rather than the run-up height. This observation could explain why both villages located on the lee-side edge of Babi Island were completely washed away by the tsunami attack.

6. Concluding remarks

In this study, we apply a 3-dimensional RANS model to the conical island run-up problem. From the numerical results and comparison with the experimental measured data, we have the following results:

1. The maximum run-up heights along the conical island are well predicted by both 2D and 3D models.

2. From the 3D model, the horizontal velocity is strongly dependent on the water depth especially at the lee side of the island. A strong vertical velocity profile is observed near the conical island and these patterns persist beyond the island.
3. Strong turbulent energy dissipation is shown on the lee side, which implies intense energy transfer from the wave to the land. This could explain why the 3D model has a stronger horizontal velocity than the 2D, but has a similar run-up height as the 2D.
4. The location at which the maximum TKE is generated is not in the lee, but in both lee-side edges of the island.From these conclusions, it can be argued that there is an obvious limitation on using depth-averaged 2D models for the simulation of run-up processes on the conical shape island. In the comparisons with observed data in the field, care must be taken to interpret 2D model results. The 3D numerical results eventually need to be compared with the physical experimental data, especially for flow pattern and turbulent intensity values. However, it could be a useful tool to verify the 2D depth-averaged model results.

Acknowledgement

This work was partly supported from tsunami R&D program of MOGAHA and MOMAF of Korean Government. It is also supported from Russian RFBR (05-05-64265) and INTAS (06-1000013-9236).

References

Briggs, M.J., Synolakis, C.E., Harkins, G.S., 1994. Tsunami runup on a conical island. Proc. of Waves — Physical and Numerical Modelling, Vancouver, Canada.

Cho, Y.S., 1995. Numerical simulations of tsunami propagation and run-up. Ph.D. Thesis, School of Civil and Env. Engrg., Cornell University, Ithaca, NY.

Cho, Y.S., Liu, P.L.-F., 1999. Crest length effects in nearshore tsunami run-up around islands. J. Geophys. Res. 104, 7907–7913.

Choi, B.H., Hong, S.J., Pelinovsky, E., 2006. Distribution of runup heights of the December 26, 2004 tsunami in the Indian Ocean. Geophys. Res. Lett. 33, L13601. doi:10.1029/2006GL025867.

Flow Science, Inc., 2002. FLOW-3D User's Manual . vols. 1 & 2.

Hirt, C.W., 1994. Weir discharge and counter currents. Proceedings 1st International Conference on Hydroinformatics. Delft. 19–23 September.

Hirt, C.W., Nichols, B.D., 1981. Volume of fluid (VOF) method for the dynamics of free boundaries. J. Comp. Physics 39, 201–225.

Hirt, C.W., Sicilian, J.M., 1985. A porosity technique for the definition of obstacles in rectangular cell meshes. Proc. Fourth International Conf. Ship Hydro. National Academy of Science, Washington, DC.

Katell, G., Eric, B., 2002. Accuracy of solitary wave generation by a piston wave maker. J. Hydraul. Res. 4 (3), 321–331.

Liu, P.L.-F., Synolakis, C., Yeh, H., 1991. A report on the international workshop on long wave runup. J. Fluid Mech. 229, 678–688.

Liu, P.L.-F., Cho, Y.S., Yoon, S.B., Seo, S.N., 1994. Numerical simulations of the 1960 Chilean tsunami propagation and inundation at Hilo, Hawaii. In: El-Sabh, M.I. (Ed.), Recent Development in Tsunami Research. Kluwer Academic Publishers.

Liu, P.L.-F., Cho, Y.S., Briggs, M.J., Kanoglu, U., Synolakis, C.E., 1995a. Run-up of solitary waves on a circular island. J. Fluid Mech. 302, 259–285.

Liu, P.L.-F., Cho, Y.S., Yoon, S.B., Seo, S.N., 1995b. Numerical simulations of the 1960 Chilean tsunami propagation and inundation at Hilo, Hawaii. In: Tsuchiya, Shuto (Eds.), Tsunami: Progress in Prediction, Disaster Prevention and Warning. Kluwer Academic Publishers, pp. 99–115.

Nichols, B.D., Hirt, C.W., Hotchkiss, R.S., 1980. SOLA-VOF: A Solution Algorithm for Transient Fluid Flow with Multiple Free Boundaries, LA-8355. Los Alamos National Laboratory.

Pelinovsky, E., Troshina, E., Golinko, V., Osipenko, N., Petrukhin, N., 1999. Runup of tsunami waves on a vertical wall in a basin of complex topography. Phys. Chem. Earth, Part B Hydrol. Oceans Atmos. 214 (5), 431–436.

Rodriguez, J.F., Bombardelli, F.A., García, M.H., Frothingham, K.M., Rhoads, B.L., Abad, J.D., 2004. High-resolution numerical simulation of flow through a highly sinuous river reach. Water Resour. Manag. 18, 177–199.

Versteeg, H.K., Malalasekera, W., 1995. An introduction to computational fluid dynamics. The Finite Volume Method. Prentice Hall, p. 257.

Yakhot, V., Orszag, S.A., 1986. Renormalization group analysis of turbulence. I. Basic theory. J. Sci. Comput. 1, 1–51.

Yeh, H., Liu, P., Synolakis, C. (Eds.), 1996. Long-wave Runup Models. World Scientific.